

Negative Allosteric Modulators That Target Human $\alpha 4\beta 2$ Neuronal Nicotinic Receptors

Brandon J. Henderson, Ryan E. Pavlovicz, Jerad D. Allen, Tatiana F. González-Cestari, Crina M. Orac, Andrew B. Bonnell, Michael X. Zhu, R. Thomas Boyd, Chenglong Li, Stephen C. Bergmeier, and Dennis B. McKay

Division of Pharmacology, College of Pharmacy (B.J.H., J.D.A., T.F.G.-C., D.B.M.), Biophysics Graduate Program (R.E.P.), and Division of Medicinal Chemistry and Pharmacognosy, College of Pharmacy (C.L.), Ohio State University, Columbus, Ohio; Department of Neuroscience, Ohio State University College of Medicine, Columbus, Ohio (A.B.B., M.X.Z., R.T.B.); and Department of Chemistry and Biochemistry, Ohio University, Athens, Ohio (C.M.O., S.C.B.)

Received April 2, 2010; accepted June 14, 2010

ABSTRACT

Allosteric modulation of neuronal nicotinic acetylcholine receptors (nAChRs) is considered to be one of the most promising approaches for therapeutics. We have previously reported on the pharmacological activity of several compounds that act as negative allosteric modulators (NAMs) of nAChRs. In the following studies, the effects of 30 NAMs from our small chemical library on both human $\alpha 4\beta 2$ (H $\alpha 4\beta 2$) and human $\alpha 3\beta 4$ (H $\alpha 3\beta 4$) nAChRs expressed in human embryonic kidney ts201 cells were investigated. During calcium accumulation assays, these NAMs inhibited nAChR activation with IC₅₀ values ranging from 2.4 μ M to more than 100 μ M. Several NAMs showed relative selectivity for H $\alpha 4\beta 2$ nAChRs with IC₅₀ values in the low micromolar range. A lead molecule, KAB-18, was identified that shows relative selectivity for H $\alpha 4\beta 2$ nAChRs. This molecule contains three phenyl rings, one piperidine ring, and one ester

bond linkage. Structure–activity relationship (SAR) analyses of our data revealed three regions of KAB-18 that contribute to its relative selectivity. Predictive three-dimensional quantitative SAR (comparative molecular field analysis and comparative molecular similarity indices analysis) models were generated from these data, and a pharmacophore model was constructed to determine the chemical features that are important for biological activity. Using docking approaches and molecular dynamics on a H $\alpha 4\beta 2$ nAChR homology model, a binding mode for KAB-18 at the α/β subunit interface that corresponds to the predicted pharmacophore is described. This binding mode was supported by mutagenesis studies. In summary, these studies highlight the importance of SAR, computational, and molecular biology approaches for the design and synthesis of potent and selective antagonists targeting specific nAChR subtypes.

Introduction

Neuronal nicotinic acetylcholine receptors (nAChRs) are ligand-gated ion channels composed of five protein subunits encoded by a family of related, but distinct, genes (Anand et al., 1991; Cooper et al., 1991). Multiple nAChR subtypes have been described based on subunit ($\alpha 2$ – $\alpha 10$ and $\beta 2$ – $\beta 4$) composi-

tion; the three most prominent native neuronal nAChR subtypes are $\alpha 4\beta 2$, $\alpha 3\beta 4$, and $\alpha 7$ (Lukas et al., 1999). nAChRs mediate fast synaptic transmission and modulate the release of several neurotransmitters (e.g., norepinephrine, serotonin, GABA, dopamine) and neurohormones (e.g., epinephrine) in many parts of the vertebrate central and peripheral nervous systems. nAChRs are associated with many physiologically important mechanisms (e.g., cognition, arousal, pain sensation, addiction) and a number of neurological diseases (e.g., depression, schizophrenia, Alzheimer's disease, Tourette's syndrome, and autism) (Lloyd and Williams, 2000; Gotti et al., 2006). However, the specific nAChR subtypes involved with most of these physiological processes or diseases are not known.

This work was supported by the National Institutes of Health National Institute on Drug Abuse [Grant DA029433]. B.J.H. was supported by the National Institutes of Health National Institute on Drug Abuse Diversity Supplement. R.E.P. was supported by the American Foundation for Pharmaceutical Education. A grant of computational resources was received from the Ohio Supercomputer Center.

Article, publication date, and citation information can be found at <http://jpet.aspetjournals.org>.
doi:10.1124/jpet.110.168211.

ABBREVIATIONS: nAChR, neuronal nicotinic acetylcholine receptor; H $\alpha 4\beta 2$, human $\alpha 4\beta 2$; H $\alpha 3\beta 4$, human $\alpha 3\beta 4$; NAM, negative allosteric modulator; LBD, ligand binding domain; MD, molecular dynamics; CoMFA, comparative molecular field analysis; CoMSIA, comparative molecular similarity indices analysis; SAR, structure–activity relationship; QSAR, quantitative SAR; GASP, genetic algorithm similarity program; HBK, HEPES-buffered Krebs; HEK, human embryonic kidney; fluo-4-AM, fluo-4-acetoxymethyl ester; DMSO, dimethyl sulfoxide; HBA, hydrogen bond acceptor.

The discovery of small molecules that target specific subtypes of nAChRs would contribute significantly to our understanding of the role specific nAChR subtypes play in normal and pathophysiological states and hold clinical promise for the treatment of several neuropathologies. Despite their obvious importance, the discovery of new drugs targeting specific nAChR subtypes has been slow. The focus of most nAChR drug discovery programs is on drugs that target orthosteric sites. One difficulty with this approach is the high degree of amino acid sequence homology among nAChR α and β subunits in the ligand binding domain for acetylcholine, making it difficult to develop drugs that specifically target nAChR subtypes. Thus, the selectivity of most nAChR drugs directed at orthosteric sites is modest at best. Looking for drugs targeting "nonorthosteric" sites of nAChRs (e.g., allosteric, noncompetitive sites) may be a more promising approach.

Allosteric binding sites are distinct from the orthosteric sites, allowing allosteric and orthosteric agents to bind simultaneously. Allosteric sites typically are defined by drugs that bind to the receptor (at nonorthosteric sites) and modulate function. Moaddel et al. (2007) described several noncompetitive, negative allosteric sites on nAChRs: central luminal sites, the ethidium binding site, and the quinacrine binding site. Several drugs bind the internal lumen of the nAChR-associated ion channel. These drugs include histrionicotoxin, phencyclidine, and mecamlamine and are often referred to as channel blockers (Changeux et al., 1986; Gallagher et al., 2001; Moaddel et al., 2007). The ethidium binding site, which also binds chlorpromazine and clozapine, was characterized through photoaffinity labeling and localized at the extracellular portion of the receptor, 46 Å above the transmembrane region (Pratt et al., 2000). The quinacrine binding site was identified within the transmembrane domain, 7 to 12 Å below the extracellular transmembrane domain interface (Arias, 1998).

We have discovered a class of nAChR NAMs that target a novel negative allosteric site on nAChRs (McKay et al., 2007; González-Cestari et al., 2009). Using our small chemical library of structurally similar NAMs, the present study describes structure–activity relationship (SAR) analyses on recombinant human $\alpha 4\beta 2$ (H $\alpha 4\beta 2$) and recombinant human $\alpha 3\beta 4$ (H $\alpha 3\beta 4$) nAChRs. 3D-QSAR [comparative molecular field analysis (CoMFA)] and comparative molecular similarity indices analysis (CoMSIA) models were generated from these data, and a pharmacophore was constructed to determine the chemical features that are important for biological activity. Using docking approaches and molecular dynamics (MD) on a homology model for the H $\alpha 4\beta 2$ nAChR, a binding mode for our lead molecule, KAB-18, at the α/β interface is described. Site-directed mutagenesis studies were designed

to validate the existence of this site on H $\alpha 4\beta 2$ nAChRs. Overall, these studies present a novel class of NAMs that show relative selectivity for H $\alpha 4\beta 2$ nAChRs. In addition, these data present the novel site of interaction for this class of NAMs on H $\alpha 4\beta 2$ nAChRs.

Materials and Methods

Materials. Fluo-4-acetoxymethyl ester (Fluo-4-AM), probenecid, and Pluronic F-127 were obtained from Molecular Probes (Eugene, OR). Dulbecco's modified Eagle medium, penicillin, streptomycin, and L-glutamine were obtained from Invitrogen (Carlsbad, CA). nAChR agonists and antagonists (Table 1) were purchased from Sigma-Aldrich (St. Louis, MO) with the exception of KAB-18. All other reagents were purchased from Thermo Fisher Scientific (Pittsburgh, PA). In general, molecules (Tables 2, 3, 4, and 5) were prepared by reaction of hydroxymethyl piperidine with the appropriate alkyl halide to provide the *N*-alkyl hydroxymethyl piperidine as reported previously (Bergmeier et al., 1999, 2004; Bryant et al., 2002; Huang et al., 2008). This molecule was then coupled to the appropriate carboxylic acid to provide the target molecule (Bergmeier et al., 2004). All molecules were >98% pure as shown by ¹H NMR, ¹³C NMR, and high-resolution mass spectrometry. All compounds were converted to their hydrochloride or oxalate salts. For pharmacological evaluation, because of solubility problems all compounds were initially dissolved in 100% DMSO (0.01 M stocks). Further dilutions of compounds were made in double distilled H₂O (≤ 100 μ M).

Calcium Accumulation Assays. A previously reported procedure that has been used for rat $\alpha 3\beta 4$ nAChRs stably expressed in HEK ts201 cells has been adapted for this work (McKay et al., 2007; González-Cestari et al., 2009). For the calcium accumulation assays, HEK ts201 cells stably expressing either H $\alpha 4\beta 2$ or H $\alpha 3\beta 4$ nAChRs (obtained from Professor Jon Lindstrom, University of Pennsylvania, Philadelphia, PA) were used. These H $\alpha 4\beta 2$ stably transfected HEK cells express predominantly low-sensitivity ($\alpha 4$)₃($\beta 2$)₂ nAChRs (Nelson et al., 2003). Cells were plated at a density of 2.0 to 2.3 $\times 10^5$ cells per well in clear 96-well culture plates coated with poly-L-ornithine. Plated cells were incubated at 37°C in 5% CO₂ in Dulbecco's modified Eagle's medium supplemented with 10% fetal bovine serum, 10 mM L-glutamine, 0.7 mg/ml G418 (Geneticin), 100 units/ml penicillin, 100 μ g/ml streptomycin, and 100 μ g/ml zeocin. Cells were used for experiments at ~100% confluence, typically 24 to 48 h after plating. On the day of the experiment, cells were washed with 100 μ l of HEPES-buffered Krebs (HBK) solution (155 mM NaCl, 4.6 mM KCl, 1.2 mM MgSO₄, 1.8 mM CaCl₂, 6 mM glucose, and 20 mM HEPES, pH 7.4) and incubated (protected from light) for 30 min at 37°C followed by 30 min at 24°C with 40 μ l of HBK containing 2 μ M fluo-4-AM solution, 2.5 mM probenecid, and 0.05% Pluronic F127. Fluo-4-AM and Pluronic F127 were dissolved in DMSO (100 and 20% w/v, respectively), resulting in a final DMSO concentration of <0.1%. After loading the cells with fluo-4-AM, the cells were washed (1 \times), and 80 μ l of HBK was added to each well. The plates were then placed into a fluid handling integrated fluorescence plate reader (FlexStation; Molecular Devices, Sunnyvale, CA). Fluo-4 fluores-

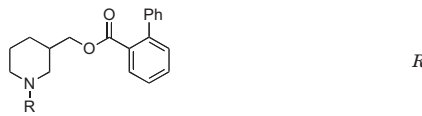
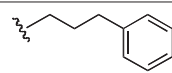
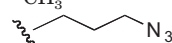
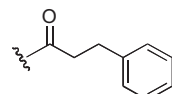
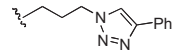
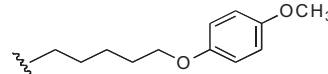
TABLE 1
Agonist and antagonist study on human nAChRs

	H $\alpha 4\beta 2$ nAChRs		H $\alpha 3\beta 4$ nAChRs	
	EC ₅₀ or IC ₅₀ Value ^a	<i>n</i> _H	EC ₅₀ or IC ₅₀ Value ^a	<i>n</i> _H
Epibatidine (EC ₅₀)	18.1 (6.5–50.6) nM	0.6	37.4 (10.7–71.4) nM	0.9
Nicotine (EC ₅₀)	8.9 (5.7–13.9) μ M	1.2	9.1 (4.5–18.6) μ M	0.9
D-tubocurarine (IC ₅₀)	2.3 (1.9–3.9) μ M	–0.7	1.6 (0.4–3.5) μ M	–0.9
Mecamylamine (IC ₅₀)	0.5 (0.3–0.8) μ M	–0.9	0.2 (0.1–0.3) μ M	–0.8
KAB-18 (IC ₅₀)	13.5 (9.7–18.5) μ M	–0.7	NA	

*n*_H, Hill coefficient; NA, no activity at concentrations up to 100 μ M.

^a Values represent geometric means (confidence limits), *n* = 4–8.

TABLE 2
Region 1 SAR studies

		H α 4 β 2 nAChRs		H α 3 β 4 nAChRs	
		IC ₅₀ Value (μ M) ^a	n _H	IC ₅₀ Value (μ M) ^a	n _H
KAB-18		13.5 (9.7–18.5)	–0.7	NA	
COB-1	–H	7.1 (5.4–9.4)	–1.1	8.1 (4.2–15.7)	–0.7
COB-3	–(CH ₃) ₂	2.4 (1.6–3.8)	–1.0	6.4 (4.4–9.3)	–0.7
COB-2	–CH ₃	6.9 (4.2–11.3)	–1.0	4.8 (2.8–8.3)	–1.2
DDR-15		4.3 (2.7–7.0)	–0.7	1.8 (0.7–5.1)	–1.1
DDR-13		5.7 (3.2–10.3)	–0.4	NA	
DDR-18		6.4 (3.7–11.1)	–1.0	NA	
APB-8		7.6 (2.0–29.0)	–0.8	22.4 (11.8–42.4)	–0.7

n_H, Hill coefficient; NA, no activity at concentrations up to 100 μ M.

^a Values represent geometric means (confidence limits), n = 4–8.

cence was read at an excitation of 494 nm and an emission of 520 nm from the bottom of the plate, and changes in fluorescence were monitored at ~1.5-s intervals. Probenecid (2.5 mM) was included in all of the solutions once the cells were loaded with fluo-4 to prevent its leakage from the cells. The experimental design involved three treatment periods (20, 40, and 60 s) and three treatment groups (control-sham treated, control-agonist treated, and antagonist treated). All groups were initially incubated in HBK, and fluorescence was monitored for 20 s. For the control-agonist treated groups, HBK (40 μ l) was then added, and the fluorescence was monitored for 40 s, followed by the addition of epibatidine (40 μ l of a 12 μ M solution) to achieve a final concentration of 3 μ M. The effects after agonist addition were monitored for 60 s. For the antagonist-treated groups, the antagonist (40 μ l of a 3 \times solution) was added, and fluorescence was monitored for 40 s, followed by the addition of epibatidine with the antagonist (at 60 s). The control-sham groups were treated with HBK during each of the treatment periods with fluorescence being monitored continuously to establish resting (background) levels of cell fluorescence. Functional responses were quantified by first calculating the net fluorescence changes (the difference between control sham-treated and control agonist-treated groups). Net peak (maximum) fluorescence values during the third treatment period for both the control-agonist treatment group and the antagonist (with agonist) treatment group were determined. Results were expressed as a percentage of control-agonist groups. Because of solubility problems, compound concentrations more than 100 μ M were not used in our concentration–response studies. The DMSO concentration at this compound concentration was 1% and had no effect on basal or agonist-induced increases in fluorescence intensity.

GASP. GASP (Genetic Algorithm Similarity Program) is a toolset of the molecular modeling program SYBYL designed for the construction of pharmacophore models. GASP uses an alignment of molecules to develop pharmacophores by using similarity constraints to optimize the orientation of molecule sets. For these alignments, the population size was set to 125, and the allele mutate weight was set to 96. The fitness increment was set to 0.02. Alignments for each set of molecules were repeated for 10 runs, and the optimal model was selected based on visual inspection. For generation of the pharmacophore model, four molecules (KAB-18, DDR-13, DDR-18, and DDR-5) were selected based on their relative selectivity for α 4 β 2 nAChRs.

CoMFA. CoMFA is a toolset of SYBYL used to evaluate 3D-QSAR. In this approach, evaluation of electrostatic and steric interactions is

correlated to biological activity for the determination of important structural features within sets of molecules. For these studies, a cutoff value of 30 kcal/mol was used. Interaction fields were built on a 2.0-Å spaced lattice and continued beyond each structure by 4.0 Å in all directions. Of the molecules used, six were selected to construct models and be used as a training set to correlate predicted and experimentally derived IC₅₀ values (see Table 7). For the test set, 11 molecules were randomly selected (see Table 8) outside of the training set. Model statistics were generated as described previously (McKay et al., 2007) where the dependent variables (biological descriptors) were IC₅₀ values generated by using the calcium accumulation assay with H α 4 β 2 nAChRs.

CoMSIA. CoMSIA is a toolset of SYBYL similar to CoMFA. CoMSIA uses Gaussian functions as opposed to Lennard-Jones potential and Coulombic potentials. The same training set and test set molecules used in the CoMFA model were selected for the CoMSIA model.

Docking and Molecular Dynamics. KAB-18 was docked to a homology model of the H α 4 β 2 LBD to determine a precise binding mode. The model was initially built with the MODELLER software in the unbound state as reported earlier (González-Cestari et al., 2009). Before docking KAB-18, epibatidine was docked to the agonist binding site so that the noncompetitive binding mode of KAB-18 could be determined. Dockings were performed with the Lamarckian genetic algorithm as implemented in AutoDock 4.0 (Morris et al., 1998). Each docking job consisted of 100 individual runs in which each run used a population size of 150 with a cutoff of 100,000,000 energy evaluations. The final docking poses were clustered with an all-atom root mean square deviation of 2 Å. MD simulations of some docking modes were evaluated to determine the stability of the ligand in the docked position. MD simulations were performed with the Amber suite of programs (Case et al., 2005). Simulation protocol involved first solvating the entire extracellular domain complex and a TIP3P water model octahedron with a 15-Å buffer around all edges, adding counterions, then energy-minimizing the system. After energy minimization, the system was simulated for 200 ps during which all protein and ligand atoms were restrained with a 50 kcal/mol harmonic potential to allow the water molecules to equilibrate around the surface of the receptor. During this equilibration stage, the temperature was increased from 0 to 300 K. After equilibration, the system was simulated at a constant 300 K with a heat bath

TABLE 3
Region 2 SAR studies

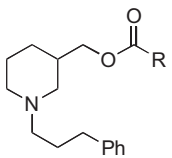
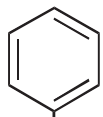
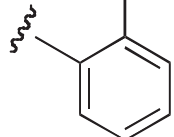
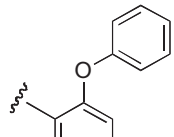
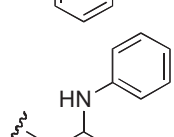
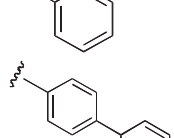
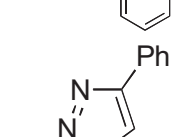
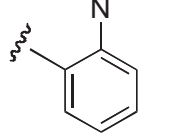
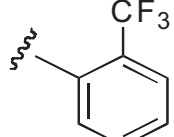
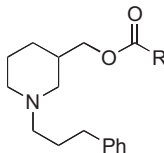
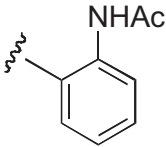
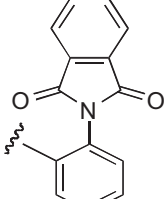
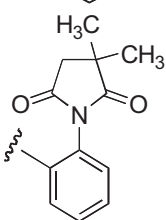
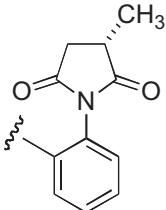
		H α 4 β 2 nAChRs		H α 3 β 4 nAChRs	
		IC ₅₀ Value (μ M) ^a	<i>n</i> _H	IC ₅₀ Value (μ M) ^a	<i>n</i> _H
KAB-18		13.5 (9.7–18.5)	–0.7	NA	
DDR-1		25.5 (17.2–37.7)	–1.1	13.2 (6.4–27.3)	–0.6
DDR-2		10.6 (3.5–32.1)	–0.7	19.5 (6.7–56.9)	–0.6
KAB-21		6.3 (1.9–20.9)	–0.9	18.5 (7.3–46.2)	–0.7
DDR-19		2.8 (1.3–6.1)	–0.9	4.3 (1.6–11.4)	–0.9
KAB-24		8.0 (4.2–15.3)	–1.2	5.5 (1.7–17.4)	–0.9
KAB-22		9.4 (5.5–16.1)	–1.3	23.1 (11.1–48.2)	–1.2
KAB-23		7.9 (4.9–12.7)	–0.7	12.1 (8.1–17.9)	–0.9

TABLE 3—Continued

	R	H α 4 β 2 nAChRs		H α 3 β 4 nAChRs	
		IC ₅₀ Value (μ M) ^a	n _H	IC ₅₀ Value (μ M) ^a	n _H
KAB-19		5.5 (2.0–15.2)	–1.1	4.3 (1.0–17.7)	–0.9
KAB-20		6.0 (4.4–8.2)	–1.5	5.9 (4.1–8.4)	–0.8
KAB-30		4.9 (2.5–9.5)	–1.5	5.0 (3.0–8.3)	–1.3
IB-2		10.5 (7.4–14.8)	–0.8	10.9 (5.1–23.3)	–0.9

n_H, Hill coefficient; NA, no activity at concentrations up to 100 μ M.

^a Values represent geometric means (confidence limits), n = 4–8.

coupling constant of 2.0 ps. All simulations were performed at a constant 1 atm with a pressure relaxation time of 2.0 ps. Nonbonded interaction calculations were cut off at 8 Å, and the electrostatic energy was computed by using the Particle Mesh Ewald method.

Site-Directed Mutagenesis and Transient Expression of α 4 β 2 nAChRs. Human nAChR α 4 and β 2 full-length cDNAs in the vector pSP64 (poly A) were obtained from Prof. Jon Lindstrom and used as the templates for mutagenesis. A single mutation was made in both the α 4 subunit and the β 2 subunit by using the QuikChange Lightning Multi Site-Directed Mutagenesis Kit (Stratagene) following the manufacturer's instructions. Primers were designed by using the QuikChange Primer Design Program (Stratagene) and Oligo 4.0 (National Biosciences, Plymouth, MN). Primers were synthesized by Invitrogen. Primers were designed to replace the α 4 amino acid with one in a similar position in the human α 3 subunit, whereas the β 2 sequence was changed to an amino acid in a similar position in the human β 4 subunit. The following complementary primers were designed to change the arginine (AGG) at position 187 in the α 4 subunit to isoleucine (ATA): α 4 mutant (+), 5'-GGGCACCTACAA-CACCATAAAGTACGAGTGTGTGC-3' and α 4 mutant (–), 5'-GCACAGCACTCGTACTTTATGGTGTGTAGGTGCC-3'. The following primer was designed to change the threonine (ACC) at position 58 in the β 2 subunit to lysine (AAG): β 2 mutant, 5'-CC-ACCAATGTCTGGCTGAAAGCAGGAGTGGGAAGATTATCG-3'. The underlined nucleotides defined the mutations. The mutant α 4 cDNA was then subcloned into the eukaryotic expression vector pcDNA

3.1+ (Invitrogen), whereas the mutant β 2 cDNA was subcloned into pcDNA 3.1+Zeo (Invitrogen). The wild-type human α 4 and β 2 cDNAs were also subcloned into the pcDNA 3.1+ and pcDNA 3.1+Zeo vectors, respectively. All cDNA clones were completely sequenced with a 3730 DNA Analyzer (Applied Biosystems, Foster City, CA) at the Ohio State University Plant-Microbe Genomics Facility. DNAs used for transfection were purified by using PureLink High Pure Mini or Midi Kits (Invitrogen). HEK ts201 cells (kind gift of Dr. Rene Anand, Ohio State University, Columbus, OH) were transiently transfected with mutant H α 4 β 2 and wild-type H α 4 β 2 cDNAs by using Lipofectamine 2000 (Invitrogen) in 60-mm dishes. After 8 h, the cells were plated into clear 96-well plates at a density of 2.6×10^5 cells per well for the intracellular calcium accumulation assays. The net peak (maximum) fluorescence values obtained with these transiently transfected cell lines (wild-type and mutant) were identical and ~77% of the net peak fluorescence values of the stably transfected cell line.

Calculations and Statistics. Functional data were calculated from the number of observations performed in triplicate. Curve fitting was performed with Prism software (GraphPad Software, Inc., San Diego, CA) using the equation for a single-site sigmoidal dose-response curve with a variable slope. Linear regression analyses were performed with Prism with the level of significance set at $p < 0.05$. EC₅₀ and IC₅₀ values are expressed as geometric means (95% confidence limits). In Table 9, when statistical analyses were performed, the t test was used.

TABLE 4
Region 3 SAR studies

	Piperidine Substitution	<i>R</i>	H α 4 β 2 nAChRs		H α 3 β 4 nAChRs	
			IC ₅₀ Value (μ M) ^a	<i>n</i> _H	IC ₅₀ Value (μ M) ^a	<i>n</i> _H
KAB-18	3-position, racemic		13.5 (9.7–18.5)	–0.7	NA	
PPB-12	3-position, (<i>S</i>)-enantiomer		17.5 (10.9–28.3)	–1.0	NA	
PPB-13	3-position, (<i>R</i>)-enantiomer		9.8 (4.4–21.6)	–0.9	NA	
IB-2	3-position, (<i>S</i>)-enantiomer		10.5 (7.2–14.8)	–0.8	10.9 (5.1–23.3)	–0.9
IB-4	3-position, (<i>R</i>)-enantiomer		9.0 (4.3–14.0)	–0.9	9.5 (5.0–17.7)	–0.9
COB-4	4-position, racemic		8.1 (2.1–30.7)	–0.8	10.5 (7.6–14.4)	–0.9

ⁿ_H, Hill coefficient; NA, no activity at concentrations up to 100 μ M.^a Values represent geometric means (confidence limits), *n* = 4–8.

Results

Lead Molecule. We had previously investigated the effects of novel NAMs on native bovine $\alpha 3\beta 4^*$ nAChRs [the asterisk indicating the possible presence of additional subunits (Lukas et al., 1999)] and recombinant rat $\alpha 3\beta 4$ nAChRs (McKay et al., 2007; González-Cestari et al., 2009). In the present studies, cell lines expressing either $H\alpha 4\beta 2$ or $H\alpha 3\beta 4$ nAChRs were used. The concentration-dependent responses to agonists (epibatidine and nicotine) and antagonists (mecamylamine and tubocurarine) are shown in Fig. 1 and Table 1. The EC_{50} values for epibatidine and nicotine on $H\alpha 4\beta 2$ nAChRs were 18.1 nM and 8.9 μ M, respectively. The IC_{50} values for mecamylamine and tubocurarine on $H\alpha 4\beta 2$ nAChRs were 0.5 and 2.3 μ M, respectively. The EC_{50} values for epibatidine and nicotine on $H\alpha 3\beta 4$ nAChRs were 37.4 nM and 9.1 μ M, respectively. The IC_{50} values for mecamylamine and tubocurarine on $H\alpha 3\beta 4$ nAChRs were 0.2 and 1.6 μ M, respectively. The pharmacology of these agonists and antagonists agree well with what has been reported previously (Wang et al., 1996; Olale et al., 1997; Stauderman et al., 1998; Nelson et al., 2001, 2003). Unlike these agonists and antagonists, our lead NAM, KAB-18, showed relative selectivity for $H\alpha 4\beta 2$ nAChRs. KAB-18 inhibited activation of $H\alpha 4\beta 2$ nAChRs (IC_{50} value 13.5 μ M) and had no inhibitory activity on $H\alpha 3\beta 4$ nAChRs at concentrations up to 100 μ M (Table 1; Fig. 1, C and D). The noncompetitive nature of this inhibitory activity is shown in Fig. 2; in the presence of KAB-18 at 30 μ M ($\sim IC_{60}$), inhibition was not surmountable with increasing concentrations of epibatidine.

NAM Alignment and Pharmacophore. Figure 3 illustrates the GASP alignment of the NAMs used for the model generation in these studies. The GASP-generated pharmacophore model (Fig. 3) featured four hydrophobic regions (HYD1, HYD2, HYD3, and HYD4) and one hydrogen bond acceptor region (HBA1). Using the information generated by our pharmacophore model, four regions were delineated to facilitate our SAR studies. Region 1 was defined as the substitution on the nitrogen moiety of the piperidine ring containing hydrophobic domain 1 (HYD1). Region 2 was defined as the ester acyl substitution containing HYD2 and HYD3. Region 3 was the piperidine ring that has been defined in the pharmacophore as the fourth hydrophobic region (HYD4). Region 4 was the linkage between regions 2 and 3, containing an ester bond with a hydrogen bond-accepting domain (HBA1).

Region 1 SAR. In this first series of experiments, the functional effects of several compounds with chemical modifications in region 1 were investigated and compared with our lead molecule, KAB-18 (Table 2). Molecules with hydrogen, methyl, or dimethyl substitutions (COB-1, COB-2, and COB-3, respectively) retained inhibitory activity on $H\alpha 4\beta 2$ nAChRs (IC_{50} values 7.1, 6.9, and 2.4 μ M, respectively) with small increases in potencies for COB-2 and COB-3. These modifications associated with COB-1, COB-2, and COB-3 resulted in a gain of activity on $H\alpha 3\beta 4$ nAChRs (IC_{50} values 8.1, 4.8, and 6.4 μ M, respectively). A carbonyl substitution on the α carbon of KAB-18 (DDR-13) in region 1 resulted in an increase in potency on $H\alpha 4\beta 2$ nAChRs and no change in relative selectivity for $H\alpha 4\beta 2$ nAChRs (i.e., no inhibitory activity on $H\alpha 3\beta 4$). The azidopropyl derivative, DDR-15, was more potent than KAB-18 on $H\alpha 4\beta 2$ nAChRs but also inhibited

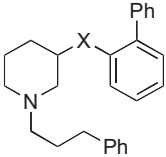
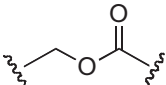
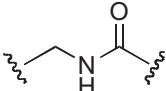
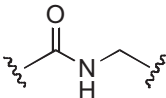
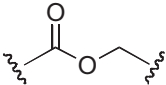
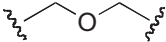
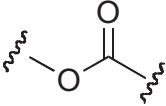
activation of $H\alpha 3\beta 4$ nAChRs. Replacement of the phenyl group of KAB-18 with a phenyl-substituted triazole (DDR-18) resulted in a slight increase in potency (IC_{50} value, 6.4 μ M), with no change in relative selectivity for $H\alpha 4\beta 2$ nAChRs. Elongation of the carbon chain of region 1 and addition of a methoxy group to the para position of the phenyl ring (APB-8) did not affect potency on $H\alpha 4\beta 2$ nAChRs; however, this modification resulted in a gain of inhibitory activity on $H\alpha 3\beta 4$ nAChRs (IC_{50} value 22.4 μ M).

Region 2 SAR. The functional effects of molecules with chemical modifications to the ester acyl component in region 2 were investigated and compared with our lead molecule, KAB-18 (Table 3). Addition of an oxygen molecule between the phenyl rings (DDR-1) resulted in a decrease in potency on $H\alpha 4\beta 2$ nAChRs and introduced inhibitory activity on $H\alpha 3\beta 4$ nAChRs (IC_{50} value 13.2 μ M). Replacement of the ether oxygen of DDR-1 with an amine (DDR-2) resulted in a slight decrease in potency for $H\alpha 4\beta 2$ nAChRs and a gain of inhibitory activity on $H\alpha 3\beta 4$ nAChRs (IC_{50} value 19.5 μ M). Moving the 2-phenyl substituent of KAB-18 to the 4-position (KAB-21) improved potency on $H\alpha 4\beta 2$ nAChRs and introduced inhibitory activity on $H\alpha 3\beta 4$ nAChRs (IC_{50} value 18.5 μ M). Addition of a triazole ring between the two phenyls (DDR-19) resulted in a 5-fold increase in potency for the $H\alpha 4\beta 2$ nAChR (IC_{50} value 2.8 μ M) but resulted in a gain of inhibitory activity on $H\alpha 3\beta 4$ nAChRs (IC_{50} value 4.3 μ M). Replacement of the phenyl with a chloride (KAB-22), methoxy (KAB-23), acetamide (KAB-19), or trifluoromethyl group (KAB-24) did not affect potency for $H\alpha 4\beta 2$ nAChRs; however, these modifications resulted in a gain of inhibitory activity on $H\alpha 3\beta 4$ nAChRs (IC_{50} values of 23.1, 12.1, 4.3, and 5.5 μ M, respectively).

Region 3 SAR. The functional effects of compounds with chemical modifications in region 3 were investigated and compared with our lead molecule, KAB-18 (Table 4). Enantiomerically pure analogs of KAB-18 (*S*)-enantiomer and (*R*)-enantiomer showed no significant change in potency or relative selectivity for $H\alpha 4\beta 2$ nAChRs compared with KAB-18. Enantiomers of succinamide-containing compounds (IB-2 and IB-4) also showed no change in potency for either nAChR subtype (Table 4) compared with KAB-18. Moving the 3-hydroxymethyl group to the 4-position (COB-4) produced a slight increase in potency on $H\alpha 4\beta 2$ nAChRs and a gain of inhibitory activity on $H\alpha 3\beta 4$ nAChRs (IC_{50} value 10.5 μ M).

Region 4 SAR. The functional effects of molecules with chemical modifications in region 4 were investigated and compared with our lead molecule, KAB-18 (Table 5). The reverse ester (JHB-9) did not affect potency for $H\alpha 4\beta 2$ nAChR; however, this modification produced a gain of inhibitory activity on $H\alpha 3\beta 4$ nAChRs (IC_{50} value 10.2 μ M). Replacement of the ester linkage with an amide linkage (DDR-5) did not affect potency on $H\alpha 4\beta 2$ nAChRs and maintained relative selectivity. The reverse ester of DDR-5 (DDR-3) did not affect potency for $H\alpha 4\beta 2$ nAChR; however, this modification produced a gain of inhibitory activity on $H\alpha 3\beta 4$ nAChRs (IC_{50} value 14.5 μ M). Shortening the linker of region 4 by using hydroxypiperidine instead of hydroxymethylpiperidine (DDR-14) produced a 2-fold increase in potency for $H\alpha 4\beta 2$ nAChRs and a gain of inhibitory activity on $H\alpha 3\beta 4$ nAChRs (IC_{50} value 2.7 μ M). Modification of the ester linkage to an ether linkage (APB-21) produced a slight decrease

TABLE 5
Region 4 SAR studies

	X	H α 4 β 2 nAChRs		H α 3 β 4 nAChRs	
		IC ₅₀ Value (μ M) ^a	n _H	IC ₅₀ Value (μ M) ^a	n _H
KAB-18		13.5 (9.7–18.5)	–0.7	NA ^c	
DDR-5		19.8 (8.3–47.1)	–0.8	NA ^c	
DDR-3		16.6 (9.7–28.6)	–0.9	14.5 (4.9–43.1)	–0.7
JHB-9		17.6 (11.6–26.8)	–0.9	10.2 (3.4–30.5)	–0.9
APB-21		12.6 (3.0–53.8)	–0.8	15.5 (8.4–29.0)	–0.9
DDR-14		6.4 (4.1–10.4)	–1.1	2.7 (0.4–17.9)	–1.2

n_H: Hill coefficient; NA, no activity at concentrations up to 100 μ M.

^a Values represent geometric means (confidence limits), n = 4–8.

in potency for the H α 4 β 2 nAChR and resulted in a gain of inhibitory activity on H α 3 β 4 nAChRs (IC₅₀ value 15.5 μ M).

Computational Modeling. NAMs were aligned by using GASP-guided subgroup alignment (Fig. 3). Subsequent 3D-

QSAR analyses (CoMFA and CoMSIA) were successfully carried out based on this alignment. The statistical significance of the CoMFA model was indicated by a cross-validated r^2 (q^2) value of 0.95 (Table 6) and a correlation coefficient (r^2) of

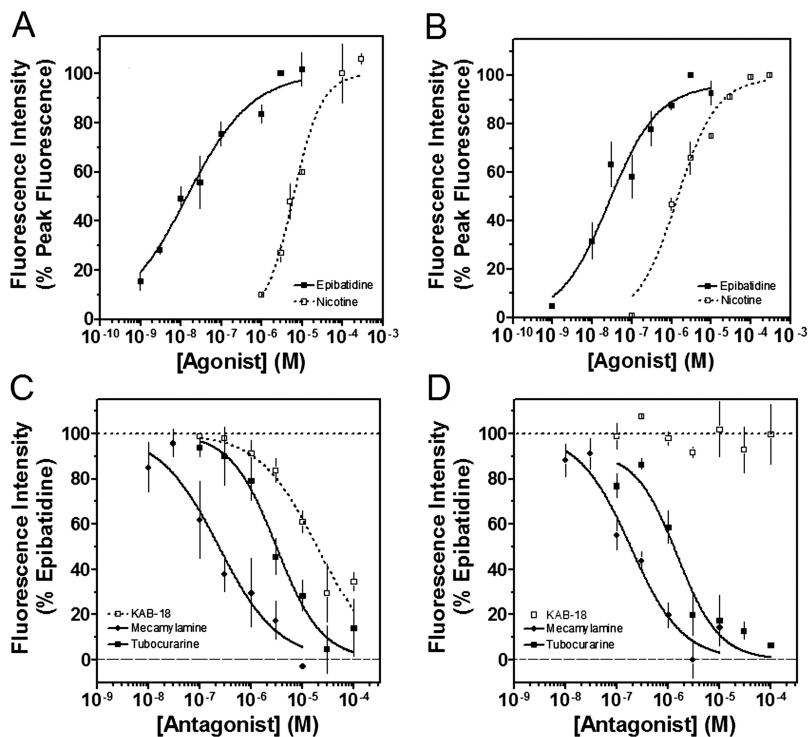


Fig. 1. Concentration–response effects of agonists, antagonists, and KAB-18 on H α 4 β 2 and H α 3 β 4 nAChRs. A and B, the concentration–response effects of nicotine (\square) and epibatidine (\blacksquare) were investigated by using HEK ts201 cells expressing H α 4 β 2 and H α 3 β 4 nAChRs. Data are expressed as a percentage of peak fluorescence responses for either 3 μ M epibatidine (epibatidine curves) or 100 μ M nicotine (nicotine curves). C and D, tubocurarine (\blacksquare), mecamylamine (\blacklozenge), and KAB-18 (\square) were investigated by using HEK ts201 cells expressing H α 4 β 2 and H α 3 β 4 nAChRs. Epibatidine (3 μ M) was used as the agonist, and data are expressed as a percentage of peak fluorescence responses for 3 μ M epibatidine. The dotted and dashed horizontal lines show the 100% control response and 100% inhibition, respectively. Values represent means \pm S.E.M.s (n = 4–10).

TABLE 6
Statistics for CoMFA and CoMSIA models

	q^2	S	% Steric	% Electrostatic	r^2 ^a	r^2 ^b
CoMFA	0.95	0.10	80	20	0.97	0.62
CoMSIA	0.87	0.02	80 ^c	20 ^d	0.97	0.81

^a Training set prediction.

^b Test set prediction.

^c Percentage of hydrophobic interaction.

^d Percentage of H-bond acceptor interaction.

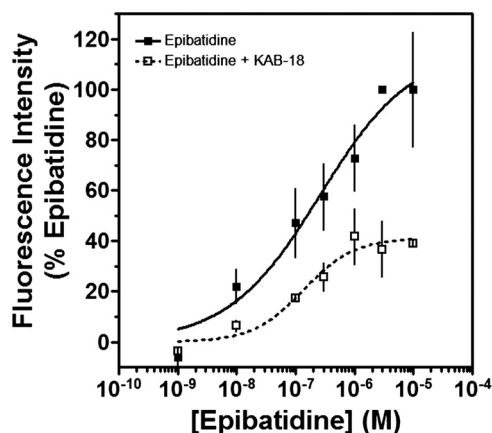


Fig. 2. Concentration–response effects of epibatidine in the absence or presence of KAB-18. The concentration–response effects of epibatidine were investigated in the absence (■) or presence (□) of 30 μ M KAB-18 by using HEK ts201 cells expressing H α 4 β 2 nAChRs. Values represent means \pm SEMs ($n = 4$).

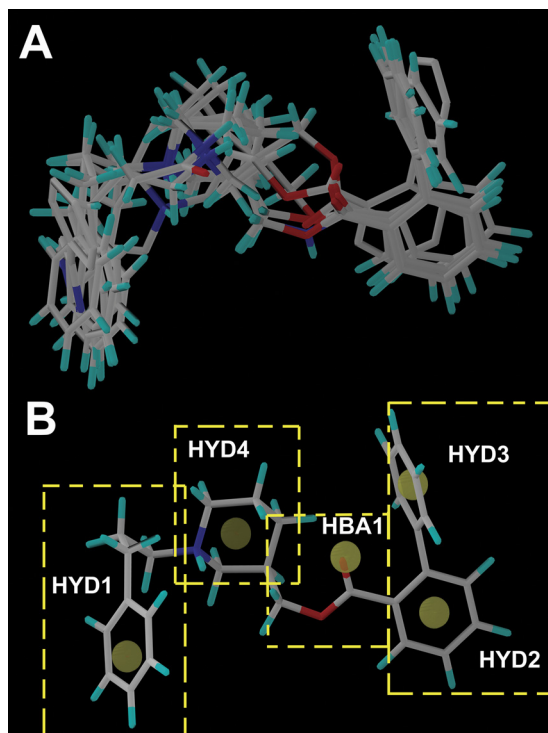


Fig. 3. Alignment of the molecules and the proposed pharmacophore targeting the negative allosteric site of the H α 4 β 2 nAChR. A, the alignment of the NAMs used in model generation is shown in capped stick representation. B, the features of the pharmacophore model generated using GASP are illustrated using KAB-18. Four hydrophobic features (HYD1, HYD2, HYD3, and HYD4) and a hydrogen bond acceptor (HBA1) feature of the pharmacophore are marked. The yellow dashed boxes outline the four regions used in the SAR studies.

TABLE 7

Comparison of predicted and experimentally derived IC₅₀ values of training set compounds

	CoMFA Log IC ₅₀ Values	CoMSIA Log IC ₅₀ Values	H α 4 β 2 nAChRs Log IC ₅₀ Values ^a
	<i>M</i>		
KAB-18	−4.94	−4.94	−4.87
DDR-13	−5.24	−5.24	−5.24
DDR-18	−5.20	−5.20	−5.19
DDR-5	−4.70	−4.70	−4.70
KAB-18(R)	−4.94	−4.94	−5.00
KAB-18(S)	−4.76	−4.76	−4.76

^a Experimentally derived data are from Tables 2–5.

0.97 (Table 6). The model's predictive power was further corroborated by the predictive value of 0.97 (r^2) when applied to the training set (Tables 6 and 7; Fig. 4). The test set resulted in a correlation coefficient (r^2) of 0.62 (Fig. 4; Table 8). The alignment of CoMFA fields with KAB-18 is shown in Fig. 5. Lead molecule KAB-18 is surrounded by yellow contours, which represents areas of steric hindrance. The green contour around the phenyl of region 2 emphasizes the importance of sterically bulky groups in this region of the binding domain, providing stabilizing hydrophobic interactions with the ligand. In a similar manner, the green contour surrounding regions 3 and 4 shows the importance of steric interactions with the piperidine ring and the phenylpropyl of region 1. The red contour surrounding the molecule emphasizes the role of a negative charge that is favorable in interaction with the positive nitrogen of the piperidine ring.

A CoMSIA model was also generated, and the predictive nature of this model was supported by the cross-validated r^2 (q^2) value of 0.87 (Table 6) and a correlation coefficient (r^2) of 0.97 (Table 6). The molecules chosen for the training set and test set in CoMFA studies were repeated for CoMSIA (Tables 7 and 8). The correlation coefficient (r^2) using the training set molecules was 0.97 (Fig. 4; Tables 6 and 7). The correlation coefficient (r^2) using the test set molecules was 0.81 (Fig. 4). When CoMSIA coefficients are plotted with lead molecule KAB-18 (Fig. 5), the yellow contours surrounding the molecule correlate with unfavorable hydrophobic interactions. The green and white contours indicate the important hydrophobic interactions with the phenyl ring of region 2 and the phenylpropyl of region 1. The blue contours suggest favorable interactions between the aromatic rings of regions 1 and 2 with positive charges in the binding pocket. The red contour near region 3 suggests the relative selectivity of less HBA in this region for biological activity.

Previously, we described potential binding sites of our NAMs using blind docking to an ensemble of rat α 3 β 4 nAChR conformations collected from an MD simulation (González-Cestari et al., 2009). A docking mode for our lead molecule, KAB-18, at the α/β interface of the H α 4 β 2 nAChR was eval-

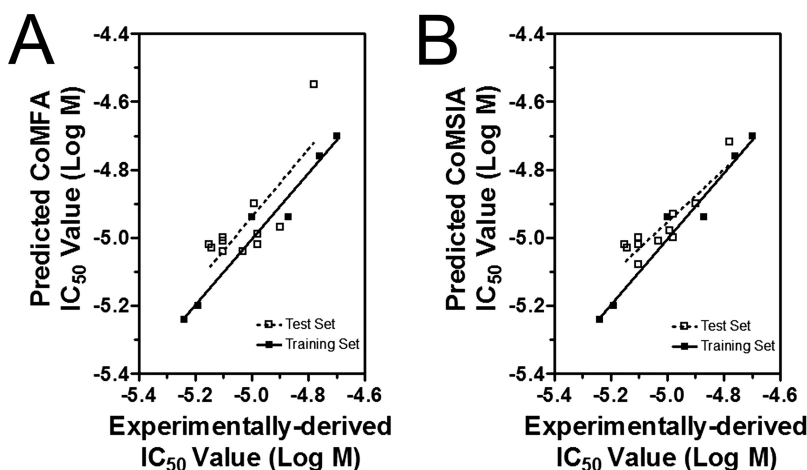


Fig. 4. Predicted and experimentally derived functional IC_{50} values of training set and test set compounds using CoMFA model (A) or CoMSIA model (B) were compared and linear regression analysis was performed. Log IC_{50} values of training set compounds are listed in Table 6, and log IC_{50} values of test set compounds are listed in Table 7.

TABLE 8
Comparison of predicted and experimentally derived IC_{50} values of analogs for test set compounds

	CoMFA Log IC_{50} Values	CoMSIA Log IC_{50} Values	H α 4 β 2 nAChRs Log IC_{50} Values ^a
<i>M</i>			
COB-1	-5.03	-5.03	-5.14
COB-2	-5.02	-5.02	-5.15
APB-8	-5.01	-5.00	-5.10
IB-2	-4.99	-5.00	-4.98
KAB-23	-5.04	-5.02	-5.10
DDR-3	-4.55	-4.72	-4.78
APB-21	-4.97	-4.90	-4.90
KAB-24	-5.00	-5.08	-5.10
DDR-2	-5.02	-4.93	-4.98
JHB-9	-4.90	-4.98	-4.99
KAB-22	-5.04	-5.01	-5.03

^a Experimentally derived data are from Tables 2–5.

uated more closely through an MD simulation. This site is adjacent to the agonist binding site (Figs. 6 and 7). KAB-18 remained stable at its docked position through the 9 ns of the simulation. Two important polar binding interactions were observed: 1) a hydrogen bond between the keto group of the ester linkage of KAB-18 and Thr58 of the β 2 subunit and 2) an interaction between the positively charged nitrogen atom of the piperidine moiety of KAB-18 and Glu60 of the β 2 subunit. After a slight induced fit in the earlier stages of the MD simulation, these interactions became stable (Fig. 6). The final binding mode of KAB-18 in the H α 4 β 2 nAChR with the hypothesized amino acid contacts is shown in Fig. 7.

Blind docking identified a binding site for KAB-18 on H α 4 β 2 nAChRs. To support interaction of KAB-18 at the predicted site, H α 4 β 2 nAChRs with a mutation in the α 4 subunit (R187I) and the β 2 subunit (T58K) were transiently expressed in HEK ts201 cells (H α 4M β 2M). These amino acids were chosen because they are proposed to be in contact with KAB-18 (Fig. 7). These mutations changed the amino acids in these positions to the cognate amino acids present in the human α 3 and β 4 subunits, respectively. Both epibatidine (agonist) and D-tubocurarine (competitive antagonist) showed no difference in apparent affinity between H α 4 β 2 WT and H α 4M β 2M nAChRs (Table 9). The noncompetitive antagonist, mecamylamine, also showed no difference in apparent affinity between H α 4 β 2 WT and H α 4M β 2M nAChRs (Table 9). KAB-18 showed a 10-fold reduction in apparent affinity ($p < 0.005$) in H α 4M β 2M nAChRs compared with

H α 4 β 2 wild-type nAChRs (Table 9). KAB-24, a negative control molecule, did not show a reduction in apparent affinity (Table 9).

Discussion

In this work, several of the effects of NAMs on human α 4 β 2 nAChRs have been characterized. Our lead molecule, KAB-18, and many of our compounds, have functional IC_{50} values in the low micromolar range. The potencies for our NAMs are similar to potencies of other established nAChR antagonists including dihydro- β -erythroidine, D-tubocurarine, tetracaine, bupropion, and mecamylamine (McKay and Sanchez, 1990; McKay and Burkman, 1993; Jensen et al., 2005). In addition, the potency of these NAMs is similar to atypical antipsychotics that act as noncompetitive inhibitors of α 4 β 2 and α 7 nAChRs (Grinevich et al., 2009). A significant finding in this study is that several of these NAMs do not inhibit H α 3 β 4 nAChRs.

SAR studies defined chemical features that contribute to the potency of our lead molecule and its relative selectivity for H α 4 β 2 nAChRs. We found that the aromatic ring and carbon chain of region 1 are important for relative selectivity on H α 4 β 2 nAChRs. Molecules with small substitutions in region 1 (COB-1, COB-2, and COB-3) were equipotent on H α 4 β 2 and H α 3 β 4 nAChRs. The addition of a carbonyl at the α carbon in region 1 of KAB-18 (DDR-13) maintains relative selectivity for H α 4 β 2 nAChRs. This substitution also increased potency (2-fold) for H α 4 β 2 nAChRs, possibly caused by additional noncovalent contacts within the allosteric binding site. DDR-13 is also unique considering that the piperidine nitrogen is uncharged because of electron resonance with the carbonyl. The relative selectivity of KAB-18 for H α 4 β 2 nAChRs is also affected by substitutions in region 2; replacement of the phenyl group of KAB-18 for smaller substituents (methoxy, chloride, acetamide, and trifluoromethyl) results in molecules (KAB-23, KAB-22, KAB-19, and KAB-24) that are equipotent on H α 4 β 2 and H α 3 β 4 nAChRs. Substitution of the aromatic ring with a succinimide ring (KAB-30, KAB-20, IB-2, and IB-4) also results in molecules that are equipotent on H α 4 β 2 and H α 3 β 4 nAChRs. These data suggest that the aromatic ring in region 2 is necessary for relative selectivity.

The ester linkage in region 4 is of interest because of susceptibility to esterases, resulting in poor drugability. We found that replacement of this ester in region 3 with an

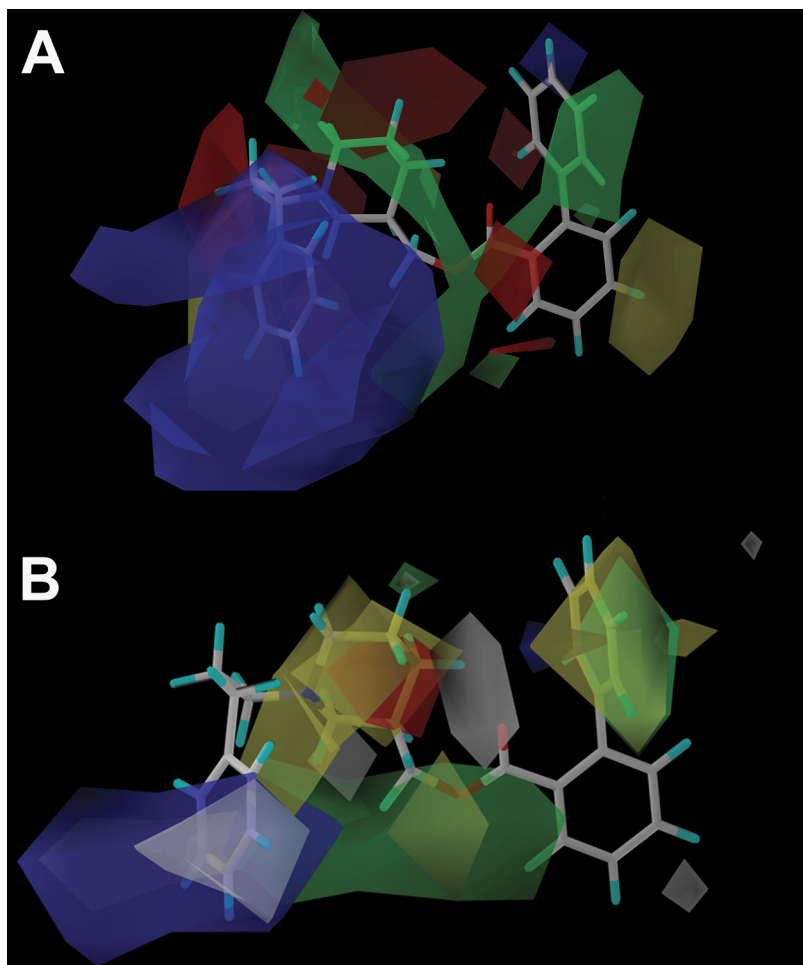


Fig. 5. CoMFA and CoMSIA models of NAM binding. A, CoMFA coefficient contours map aligned with KAB-18. The contours of the steric map are shown in yellow and green, and the contours of the electrostatic map are shown in red and blue. Greater potency (lower IC_{50} values) is correlated with less bulk near yellow, more bulk near green, more negative charge near red, and more positive charge near blue. B, CoMSIA contours aligned with KAB-18. The contours of the hydrophobic map are shown in white, yellow, and green, and the contours of the HBA map are shown in red and blue. Greater potency (lower IC_{50} values) is correlated with less bulk near yellow, more bulk near green and white, more HBA near blue, and less HBA near red.

amide (DDR-5) does not affect either potency or relative selectivity. Another finding is the importance of the orientation of the carbonyl group in region 4. Molecules with the carbonyl adjacent to the benzene ring of region 2 (KAB-18 and DDR-5) maintain relative selectivity for $H\alpha 4\beta 2$ nAChRs;

however, molecules with the reverse ester (JHB-9 and DDR-3) are equipotent on $H\alpha 4\beta 2$ and $H\alpha 3\beta 4$ nAChRs. In addition, replacement of the ester linkage with an ether linkage (APB-21) does not affect potency but relative selectivity for $H\alpha 4\beta 2$ nAChRs is lost. This may be caused by

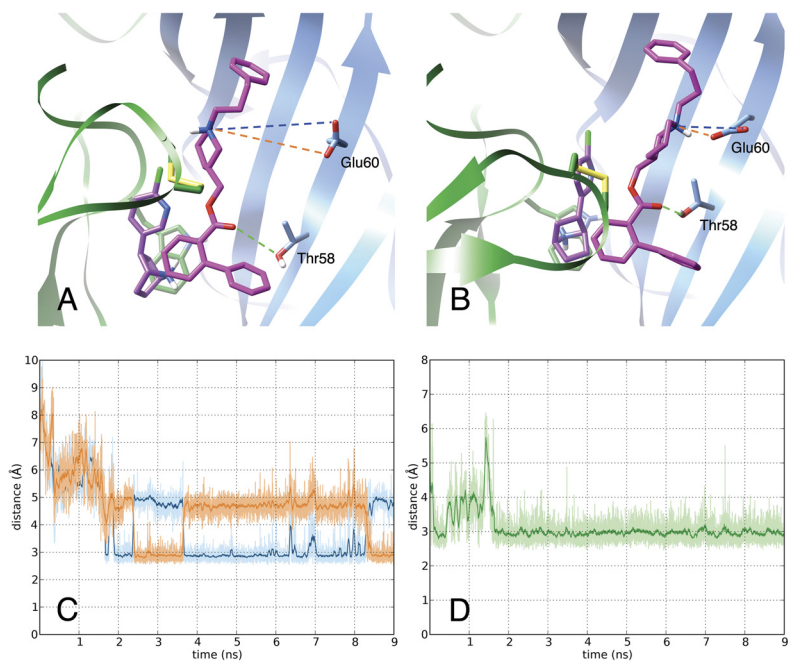


Fig. 6. Stability of KAB-18 at its proposed binding site. A and B, MD simulation of the $H\alpha 4\beta 2$ model was used to demonstrate initial docking mode (A) and induced binding mode at 7 ns (B) of KAB-18 (magenta) to the epibatidine-bound (purple) interface of the $H\alpha 4$ (green ribbon) and $H\beta 2$ (blue ribbon) subunits. Dotted lines identify key polar interactions between the ligand and the receptor. C and D, interatomic distances over time between the nitrogen of the positively charged piperidine and the two oxygen atoms of $\beta 2$ Glu60 (orange and blue labeling) and the keto group of the ester linkage and the hydroxyl-oxygen of $\beta 2$ Thr58 (green labeling), respectively.

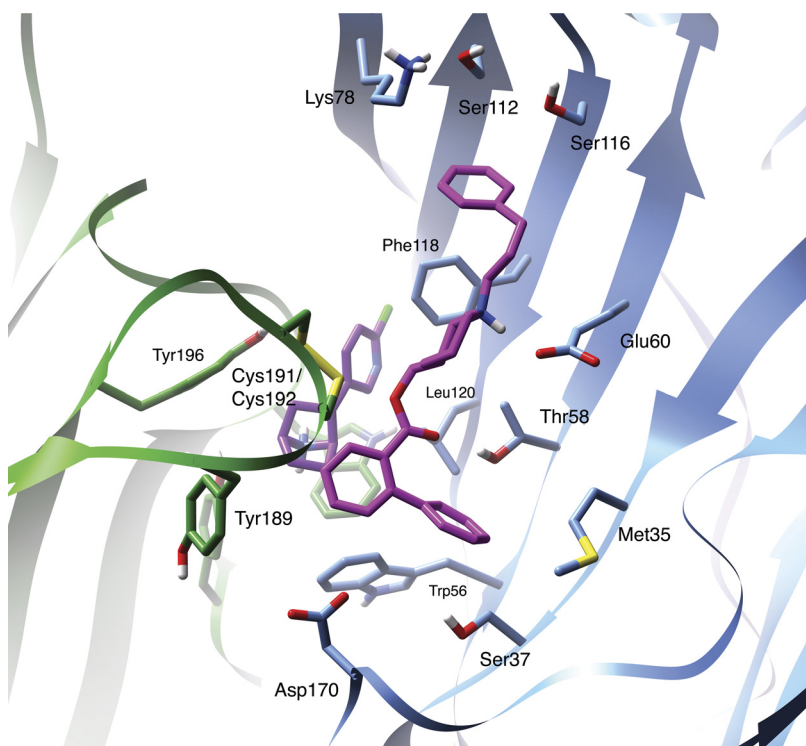


Fig. 7. Identification of ligand–receptor contacts of KAB-18 in the H α 4 β 2 nAChR model. A snapshot at 7.0 ns from MD simulation shows the induced binding mode of KAB-18 (magenta) to the epibatidine-bound (purple) interface of the H α 4 (green ribbon) and H β 2 (blue ribbon) subunits. Key amino acids contributing to the binding of KAB-18 are shown as stick figures.

TABLE 9
Effects of agonists and antagonists on wild-type and mutant human α 4 β 2 nAChRs
Values represent geometric means (confidence limits), $n = 5$ –7.

	Wild-Type H α 4 β 2 nAChRs		Mutant H α 4 β 2 nAChRs	
	EC ₅₀ or IC ₅₀ Values	n_H	EC ₅₀ or IC ₅₀ Values	n_H
Epibatidine (EC ₅₀)	36.8 (25.4–53.4) nM	0.9	34.7 (21.4–56.2) nM	1.1
D-tubocurarine (IC ₅₀)	5.5 (3.4–9.0) μ M	–1.0	7.6 (5.6–10.5) μ M	–0.8
Mecamylamine (IC ₅₀)	0.2 (0.1–0.3) μ M	–1.4	0.2 (0.1–0.4) μ M	–1.1
KAB-18 (IC ₅₀)	10.0 (5.5–18.0) μ M	–1.2	110 (80.4–150) μ M ^a	–0.6
KAB-24 (IC ₅₀)	5.9 (3.8–9.2) μ M	–1.1	9.7 (5.4–17.5) μ M	–1.2

n_H , Hill coefficient.

^a Significant difference, $P < 0.0001$.

additional geometries that are available in the ether that are not present in either the amide or ester or important hydrogen bonding interaction in the LBD. Regardless, these data support the importance of the carbonyl in region 4.

A clear disadvantage of targeting noncompetitive, allosteric sites is the limited knowledge of the binding site. To address this problem, ligand-based computational modeling was used to delineate information of this novel site on human nAChRs. CoMFA and CoMSIA models were constructed by using a set of molecules that showed relative selectivity for H α 4 β 2 nAChRs. A critical factor for proper implementation of CoMFA models lies in the precise structural alignment (Cramer, 2003). For several of the molecules in this study, precise alignment was made difficult because of structural differences. The results of the test set correlation show that CoMFA is not as suitable compared with our CoMSIA model. The CoMSIA model emphasizes the importance of both steric and hydrophobic interactions surrounding regions 1 and 2. These data are in agreement with data obtained from SAR studies, which showed that both regions were important for relative selectivity on H α 4 β 2 nAChRs.

In addition to the ligand-based approaches, structure-based approaches were used to help define the NAM binding

site. Using docking and MD simulation on the H α 4 β 2 nAChR homology model, we identified a novel binding site for KAB-18 within 10 Å from the agonist binding site at the interface of the α and β subunits; however, the interacting amino acids are primarily on the β subunit. Other allosteric sites have been reported (i.e., galantamine) for nAChRs on non- α subunits (Iorga et al., 2006; Hansen and Taylor, 2007). The docking position of KAB-18 in the H α 4 β 2 nAChR model corresponds well to the predicted pharmacophore. The pharmacophore, CoMSIA, and CoMFA models predict four favorable hydrophobic interactions between the ligand and receptor that can be mapped as follows: 1) β 4Phe118 and β 4Lys78 for HYD1; 2) α 4Cys191 and α 4Cys192, β 4Trp61 and β 4Leu120 for HYD2; 3) β 4Met35, β 4Trp61, and β 4Leu120 for HYD3; and 4) α 4Cys191 and α 4Cys192, β 4Phe118 and β 4Thr58 for HYD4. The β 4Thr58 is the hydrogen bond donor. The pharmacophore, CoMFA, and CoMSIA models predict a favorable interaction between a positively charged region and the region 1 phenyl group of KAB-18. This interaction can be mapped to β 4Lys78 in the predicted binding mode.

To determine the importance of the amino acids identified from the homology modeling studies, two amino acids of the H α 4 β 2 nAChR in close contact with KAB-18 were chosen for

mutation to their cognate amino acids found in the $\text{H}\alpha\beta\beta\text{4}$ nAChR ($\alpha\text{4 R187I} + \beta\text{2 T58K}$). We hypothesized that if the selected amino acids interacted with KAB-18, a loss of apparent affinity should be observed. Similar approaches have been reported to validate amino acids identified through models (Selent et al., 1992; Pepin et al., 1997). The functional studies showed a 10-fold reduction in apparent affinity of KAB-18 for the mutant nAChR. These data support the location of these amino acid residues within the allosteric LBD and that the homology model studies identified the NAM's binding site. To further validate the binding of this class of NAMs to this site, a molecule that was proposed to have no interaction with the mutated amino acids, KAB-24, was chosen. KAB-24 showed no difference in apparent affinity between the wild-type and mutant $\alpha\text{4}\beta\text{2}$ nAChRs (Table 9).

The computed binding mode of KAB-18 to the $\alpha\text{4}\beta\text{2}$ nAChR homology model may explain the selectivity for $\text{H}\alpha\text{4}\beta\text{2}$ nAChRs over $\text{H}\alpha\text{3}\beta\text{4}$ nAChRs. All pharmacophore features important for selectivity for $\text{H}\alpha\text{4}\beta\text{2}$ nAChRs are at positions that come into contact with amino acids that are not conserved between the two subtypes. All of these positions occur on the β subunit. In region 1, Ser112 and Lys78 of the β2 subunit exist as an arginine and isoleucine, respectively, at the corresponding site of the β4 subunit. In region 2, a Met35 exists as a glutamine at the corresponding site of the β4 subunit, whereas in regions 3 and 4 Thr58 and Phe118 exist as a lysine and leucine, respectively, at their corresponding sites of the β4 subunit. These residues may play a role in the preferential binding of particular compounds to the $\text{H}\alpha\text{4}\beta\text{2}$ nAChRs. Our computed binding mode may also explain the species differences observed with KAB-18 (González-Cestari et al., 2009). KAB-18 has been shown to inhibit rat $\alpha\text{3}\beta\text{4}$ nAChRs while having no activity on $\text{H}\alpha\text{3}\beta\text{4}$ nAChRs. Our homology models show amino acid differences between human and rat in the NAM binding site on $\alpha\text{3}\beta\text{4}$ nAChRs that potentially influence binding affinities: a Gln (human) versus Glu (rat) at β4 position 35 and a Leu (human) versus Gln (rat) at β4 position 118. Site-directed mutagenesis studies would need to be performed to validate this hypothesis, as done by Young et al. (2007) where similar observations were made with the compound TMAQ [5-(trifluoromethyl)-6-(1-methyl-azepan-4-yl)-methyl-1*H*-quinolin-2-one].

The discovery of selective antagonists of $\text{H}\alpha\text{4}\beta\text{2}$ nAChRs has important implications for the treatment of nicotine addiction. Worldwide, tobacco smoking is the leading cause of preventable death. Current pharmacotherapies [e.g., nicotine replacement therapy, antidepressant therapy and varenicline (Chantix)] have limited success and are associated with marked side effects, probably associated with off-target activities. Additional treatment strategies for nicotine addiction are needed, and the discovery of selective nAChR antagonists that target $\text{H}\alpha\text{4}\beta\text{2}$ nAChRs may provide a novel approach for smoking cessation. Mecamylamine (nonselective, noncompetitive antagonist) has shown clinical promise for nicotine cessation when coapplied with nicotine patches (Rose et al., 1994, 1998); however, mecamylamine's usage is limited because of side effects, probably linked to its nonselectivity for nAChR subtypes (Papke et al., 2001). Recently, NAMs have been shown to block nicotine reinforcement (Yoshimura et al., 2007; Hall et al., 2010). The studies presented here characterize functional activity of a novel NAM with selectivity for $\text{H}\alpha\text{4}\beta\text{2}$ nAChRs over $\text{H}\alpha\text{3}\beta\text{4}$ nAChRs and pro-

vide insight into important structural features and binding modes, contributing to the relative selectivity of our NAMs for $\text{H}\alpha\text{4}\beta\text{2}$ nAChRs. This work also documents the importance of SAR and ligand-based and structure-based computational modeling approaches for the discovery of NAMs targeting specific nAChR subtypes.

Acknowledgments

We thank Dr. Jon M. Lindstrom (Department of Neuroscience School of Medicine, University of Pennsylvania, Philadelphia) for stably transfected human cell lines and human nAChR α4 and β2 cDNAs and Dr. Rene Anand (Department of Neuroscience, College of Medicine, Ohio State University, Columbus, OH) for HEK ts201 cells.

References

- Anand R, Conroy WG, Schoepfer R, Whiting P, and Lindstrom J (1991) Neuronal nicotinic acetylcholine receptors expressed in *Xenopus* oocytes have a pentameric quaternary structure. *J Biol Chem* **266**:11192–11198.
- Arias HR (1998) Binding sites for exogenous and endogenous non-competitive inhibitors of the nicotinic acetylcholine receptor. *Biochim Biophys Acta* **1376**:173–220.
- Bergmeier SC, Ismail KA, Arason KM, McKay S, Bryant DL, and McKay DB (2004) Structure activity studies of ring E analogues of methyllycaconitine. Part 2: synthesis of antagonists to the $\alpha\text{3}\beta\text{4}$ nicotinic acetylcholine receptors through modifications to the ester. *Bioorg Med Chem Lett* **14**:3739–3742.
- Bergmeier SC, Lapinsky DJ, Free RB, and McKay DB (1999) Ring E analogs of methyllycaconitine (MLA) as novel nicotinic antagonists. *Bioorg Med Chem Lett* **9**:2263–2266.
- Bryant DL, Free RB, Thomasy SM, Lapinsky DJ, Ismail KA, McKay SB, Bergmeier SC, and McKay DB (2002) Structure-activity studies with ring E analogues of methyllycaconitine on bovine adrenal $\alpha\text{3}\beta\text{4}$ nicotinic receptors. *Neurosci Res* **42**:57–63.
- Case DA, Cheatham TE 3rd, Darden T, Gohlke H, Luo R, Merz KM Jr, Onufriev A, Simmerling C, Wang B, and Woods RJ (2005) The Amber biomolecular simulation programs. *J Comput Chem* **26**:1668–1688.
- Changeux JP, Pinset C, and Ribera AB (1986) Effects of chlorpromazine and phencyclidine on mouse α2 acetylcholine receptor kinetics. *J Physiol* **378**:497–513.
- Cooper E, Couturier S, and Ballivet M (1991) Pentameric structure and subunit stoichiometry of a neuronal nicotinic acetylcholine receptor. *Nature* **350**:235–238.
- Cramer RD (2003) Topomer CoMFA: A design methodology for rapid lead optimization. *J Med Chem* **46**:374–388.
- Gallagher MJ, Chiara DC, and Cohen JB (2001) Interactions between 3-(trifluoromethyl)-3-(m -[^{125}I] iodophenyl) diazine and tetracaine, phencyclidine, or histriocytotoxin in the *torpedo* species nicotinic acetylcholine receptor ion channel. *Mol Pharmacol* **59**:1514–1522.
- González-Cestari TF, Henderson BJ, Pavlovicz RE, McKay SB, El-Hajj RA, Pulipaka AB, Orac CM, Reed DD, Boyd RT, Zhu MX, et al. (2009) Effect of novel negative allosteric modulators of neuronal nicotinic receptors on cells expressing native and recombinant nicotinic receptors: implications for drug discovery. *J Pharmacol Exp Ther* **328**:504–515.
- Gotti C, Riganti L, Vailati S, and Clementi F (2006) Brain neuronal nicotinic receptors as new targets for drug discovery. *Curr Pharm Des* **12**:407–428.
- Grinevich VP, Papke RL, Lippello PM, and Bencherif M (2009) Atypical antipsychotics as noncompetitive inhibitors of $\alpha\text{4}\beta\text{2}$ and α7 neuronal nicotinic receptors. *Neuropharmacology* **57**:183–191.
- Hall BJ, Pearson LS, and Buccafusco JJ (2010) Effect of administration of the nicotinic acetylcholine receptor antagonist BTMPS, during nicotine self-administration, on lever responding induced by context long after withdrawal. *Neuropharmacology* **58**:429–435.
- Hansen SB and Taylor P (2007) Galanthamine and non-competitive inhibitor binding to ACh-binding protein: evidence for a binding site on non- α -subunit interfaces of heteromeric neuronal nicotinic receptors. *J Mol Biol* **369**:895–901.
- Huang J, Orac CM, McKay S, McKay DB, and Bergmeier SC (2008) The synthesis of 5-substituted ring E analogs of methyllycaconitine via the Suzuki-Miyaura cross-coupling reaction. *Bioorg Med Chem* **16**:3816–3824.
- Iorga B, Herlem D, Barré E, and Guillou C (2006) Acetylcholine nicotinic receptors: finding the putative binding site of allosteric modulators using the “blind docking” approach. *J Mol Model* **12**:366–372.
- Jensen AA, Frølund B, Liljefors T, and Krosgaard-Larsen P (2005) Neuronal nicotinic acetylcholine receptors: structural revelations, target identifications, and therapeutic inspirations. *J Med Chem* **48**:4705–4745.
- Lloyd GK and Williams M (2000) Neuronal nicotinic acetylcholine receptors as novel drug targets. *J Pharmacol Exp Ther* **292**:461–467.
- Lukas RJ, Changeux JP, Le Novère N, Albuquerque EX, Balfour DJ, Berg DK, Bertrand D, Chiappinelli VA, Clarke PB, Collins AC, et al. (1999) International Union of Pharmacology. XX. Current status of the nomenclature for nicotinic acetylcholine receptors and their subunits. *Pharmacol Rev* **51**:397–401.
- McKay DB and Burkman AM (1993) Nicotinic and non-nicotinic receptor-mediated actions of vlnblastine. *Proc Soc Exp Biol Med* **203**:372–376.
- McKay DB and Trent-Sanchez P (1990) Effect of noncompetitive nicotinic receptor blockers on catecholamine release from cultured adrenal chromaffin cells. *Pharmacology* **40**:224–230.
- McKay DB, Chang C, González-Cestari TF, McKay SB, El-Hajj RA, Bryant DL, Zhu MX, Swaan PW, Arason KM, Pulipaka AB, et al. (2007) Analogs of methyllyca-

- conitine as novel noncompetitive inhibitors of nicotinic receptors: pharmacological characterization, computational modeling, and pharmacophore development. *Mol Pharmacol* **71**:1288–1297.
- Moaddel R, Jozwiak K, and Wainer IW (2007) Allosteric modifiers of neuronal nicotinic acetylcholine receptors: new methods, new opportunities. *Med Res Rev* **27**:723–753.
- Morris GM, Goodsell DS, Halliday RS, Huey R, Hart WE, Belew RK, and Olson AJ (1998) Automated docking using a Lamarckian genetic algorithm and empirical binding free energy function. *J Comput Chem* **19**:1639–1662.
- Nelson ME, Kuryatov A, Choi CH, Zhou Y, and Lindstrom J (2003) Alternate stoichiometries of $\alpha 4\beta 2$ nicotinic acetylcholine receptors. *Mol Pharmacol* **63**:332–341.
- Nelson ME, Wang F, Kuryatov A, Choi CH, Gerzanich V, and Lindstrom J (2001) Functional properties of human nicotinic AChRs expressed by IMR-32 neuroblastoma cells resemble those of $\alpha 3\beta 4$ AChRs expressed in permanently transfected HEK cells. *J Gen Physiol* **118**:563–582.
- Olale F, Gerzanich V, Kuryatov A, Wang F, and Lindstrom J (1997) Chronic nicotine exposure differentially affects the function of human $\alpha 3$, $\alpha 4$, and $\alpha 7$ neuronal nicotinic receptor subtypes. *J Pharmacol Exp Ther* **283**:675–683.
- Papke RL, Sanberg PR, and Shytle RD (2001) Analysis of mecamylamine stereoisomers on human nicotinic receptor subtypes. *J Pharmacol Exp Ther* **297**:646–656.
- Pepin MC, Yue SY, Roberts E, Wahlestedt C, and Walker P (1997) Novel “restoration of function” mutagenesis strategy to identify amino acids of the δ -opioid receptor involved in ligand binding. *J Biol Chem* **272**:9260–9267.
- Pratt MB, Pedersen SE, and Cohen JB (2000) Identification of the sites of incorporation of [3H] ethidium diazide within the torpedo nicotinic acetylcholine receptor ion channel. *Biochemistry* **39**:11452–11462.
- Rose JE, Behm FM, Westman EC, Levin ED, Stein RM, and Ripka GV (1994) Mecamylamine combined with nicotine skin patch facilitates smoking cessation beyond nicotine patch treatment alone. *Clin Pharmacol Ther* **56**:86–99.
- Rose JE, Behm FM, and Westman EC (1998) Nicotine-mecamylamine treatment for smoking cessation: the role of pre-cessation therapy. *Exp Clin Psychopharmacol* **6**:331–343.
- Selent U, Rüter T, Köhler E, Liedtke M, Thielking V, Alves J, Oelgeschläger T, Wolfes H, Peters F, and Pingoud A (1992) A site-directed mutagenesis study to identify amino acid residues involved in the catalytic function of the restriction endonuclease EcoRV. *Biochemistry* **31**:4808–4815.
- Stauderman KA, Mahaffy LS, Akong M, Veliçelebi G, Chavez-Noriega LE, Crona JH, Johnson EC, Elliott KJ, Gillespie A, Reid RT, et al. (1998) Characterization of human recombinant neuronal nicotinic acetylcholine receptors subunit combinations of $\alpha 2\beta 4$, $\alpha 3\beta 4$ and $\alpha 4\beta 4$ stably expressed in HEK293 cells. *J Pharmacol Exp Ther* **284**:777–789.
- Wang F, Gerzanich V, Wells GB, Anand R, Peng X, Keyser K, and Lindstrom J (1996) Assembly of human neuronal nicotinic receptor $\alpha 5$ subunits with $\alpha 3$, $\beta 2$, and $\beta 4$ subunits. *J Biol Chem* **271**:17656–17665.
- Yoshimura RF, Hogenkamp DJ, Li WY, Tran MB, Belluzzi JD, Whittmore ER, Leslie FM, and Gee KW (2007) Negative allosteric modulation of nicotinic acetylcholine receptors blocks nicotine self-administration in rats. *J Pharmacol Exp Ther* **323**:907–915.
- Young GT, Broad LM, Zwart R, Astles PC, Bodkin M, Sher E, and Millar NS (2007) Species selectivity of a nicotinic acetylcholine receptor agonist is conferred by two adjacent extracellular $\beta 4$ amino acids that are implicated in the coupling of binding to channel gating. *Mol Pharmacol* **71**:389–397.

Address correspondence to: Dr. Dennis B. McKay, Division of Pharmacology, Ohio State University College of Pharmacy, 500 West 12th Avenue, Columbus, OH 43210. E-mail: mckay.2@osu.edu
